Nitric Oxide 77 (2018) 26–34

Contents lists available at ScienceDirect

Nitric Oxide

journal homepage: www.elsevier.com/locate/yniox

Characterization of human triosephosphate isomerase S-nitrosylation

Jorge Miguel Romero*, María Elena Carrizo, Juan Agustín Curtino

Centro de Investigaciones en Química Biológica de Córdoba (CIQUIBIC, Universidad Nacional de Córdoba - Consejo Nacional de Investigaciones Científicas y Técnicas (UNC-CONICET)), Departamento de Química Biológica Ranwel Caputto, Facultad de Ciencias Químicas, Universidad Nacional de Córdoba, X5000HUA, Córdoba, Argentina

ARTICLE INFO

Keywords:
Triosephosphate isomerase
S-nitrosylation
Nitric oxide
S-nitrosocysteine
S-nitrosoglutathione

ABSTRACT

Triosephosphate isomerase (TPI), the glycolytic enzyme that catalyzes the isomerization of dihydroxyacetone phosphate (DHAP) to glyceraldehyde-3-phosphate (G3P), has been frequently identified as a target of S-nitrosylation by proteomic studies. However, the effect of S-nitrosylation on its activity has only been explored in plants and algae. Here, we describe the *in vitro* S-nitrosylation of human TPI (hTPI), and the effect of the modification on its enzymatic parameters. NO-incorporation into the enzyme cysteine residues occurred by a time-dependent S-transnitrosylation from both, S-nitrosocysteine (CySNO) and S-nitrosoglutathione (GSNO), with CySNO being the more efficient NO-donor. Both X-ray crystal structure and mass spectrometry analyses showed that only Cys217 was S-nitrosylated. hTPI S-nitrosylation produced a 30% inhibition of the Vmax of the DHAP conversion to G3P, without affecting the Km for DHAP. This is the first study describing features of human TPI S-nitrosylation.

1. Introduction

Nitric oxide (NO) is a diatomic gaseous free radical produced by the NO synthase (NOS). In mammals, there are three isoforms of the enzyme: nNOS or type 1, which is expressed in the nervous system; iNOS or type 2, expressed by macrophages; and eNOS or type 3, expressed constitutively in several tissues [1]. iNOS is induced by proinflammatory cytokines such as tumor necrosis factor α and interferon-γ [2].

The biological role of NO will depend on the NOS responsible for its production. While nNOS and eNOS release NO in a controlled manner to either, up- or down-regulate biological functions in physiological events, iNOS produces large amounts of NO on the target tissue exerting toxic effects during inflammatory processes [3]. In all cases, one of the major consequences of NO release is protein S-nitrosylation, consisting of the reversible covalent attachment of NO to protein cysteine residues that could produce alterations in their function [4,5].

The mechanism by which NO produces protein S-nitrosylation in target cells is unclear. Once synthesized, NO can react with oxygen and superoxide to give reactive nitrogen species such as dinitrogen trioxide (N_2O_3) and peroxynitrite ($ONOO^-$) [6,7]. In addition, these species can react with both thiol proteins and non-thiol proteins such as glutathione and cysteine to give protein and non-protein S-nitrosothiols [5,8]. Both N_2O_3 and $ONOO^-$ as well as the non-protein S-nitrosothiols were proposed as mediators of paracrine protein S-nitrosylation [9]. $ONOO^-$ is a highly reactive S-nitrosylating agent [10] having a $t_{1/2}$ of less than 1 s. Due to its short life, this species is not a viable intercellular S-nitrosylating agent since it is only able to reach targets in its close proximity [11–13]. S-nitrosoglutathione (GSNO), S-nitrosocysteine (CySNO) and N_2O_3, being relatively more stable, become candidates for spreading the modification to other cells. On the other hand, some selectivity of protein cysteine residues to NO donors has been observed [14] although the molecular basis of this selectivity is still unknown. The effects of this posttranslational modification on different types of proteins have been reported, including: enzymes involved in mitochondrial respiration [15], transcription factors [16] and membrane receptors [17], which makes S-nitrosylation a very interesting tool to structurally study the regulations of protein function.

TPI is a glycolytic enzyme that catalyzes the isomerization of dihydroxyacetone phosphate (DHAP) to glyceraldehyde-3-phosphate (G3P), and is found in almost all organisms. Human TPI (hTPI) is a homodimeric enzyme possessing five cysteine residues per subunit, none of which is directly involved in the catalytic site. Full activity was reported for the dimeric form despite the fact that each monomer has a

Abbreviations: TPI, triosephosphate isomerase; G3P, glyceraldehyde-3-phosphate; DHAP, dihydroxyacetone; GAPDH, glyceraldehyde-3-phosphate dehydrogenase; CySNO, S-nitrosocysteine; GSNO, S-nitrosoglutathione; NEM, N-ethylmaleimide; NOS, NO synthase

* Corresponding author. Centro de Investigaciones en Química Biológica de Córdoba (CIQUIBIC), Departamento de Química Biológica Ranwel Caputto, Facultad de Ciencias Químicas, UNC-CONICET, Haya de la Torre s/n, Pabellón Argentina Ala Oeste, X5000HUA, Córdoba, Argentina.

E-mail address: jromero@fcq.unc.edu.ar (J.M. Romero).

https://doi.org/10.1016/j.niox.2018.04.004
Received 9 November 2017; Received in revised form 10 April 2018; Accepted 16 April 2018
Available online 17 April 2018
1089-8603/

complete set of catalytic residues [18]. hTPI as well as TPI from other organisms has been found to be a target of S-nitrosylation [19–25]. However, there are no studies relating to the sites and mechanism of this modification, or its effect on the human enzyme. In view of the occurrence of nitrosative stress in several disorders and the key role of TPI in glucose metabolism, it is of crucial importance to ascertain the influence of this modification on protein properties. In the present study, we analyze for the first time, the reactivity of recombinant hTPI to different NO donors and the effect of this modification on enzyme activity. In addition, we have crystallized S-nitrosylated hTPI enabling us to determine the target cysteine residue of S-nitrosylation. The results demonstrated the following:

- hTPI is S-nitrosylated by direct transfer of the nitrosonium moiety (NO^+) from CySNO and GSNO, whereas no modification was observed when the enzyme was exposed to a NO releaser compound.
- X-ray diffraction studies enabled us to detect a NO moiety only in Cys217.
- S-nitrosylation inhibited the activity of hTPI by about 30%, a value similar to that observed in the S-nitrosylated *Chlamydomonas reinhardtii* TPI.

This study is relevant to understanding the possible effects that S-nitrosylation upon nitrosative stress could have on a key enzyme of the glycolytic pathway, in disorders characterized by excessive NO production.

2. Materials and methods

2.1. Chemicals

Ascorbic acid, L-cysteine, 5,5′-dithiobis(2-nitrobenzoic acid) (DTNB or Ellman's reagent), β-Nicotinamide adenine dinucleotide (NAD), L-glutathione, Spermine NONOate, L-cysteine and Dihydroxyacetone phosphate (DHAP), were purchased from Sigma. Sodium azide was obtained from J.T. Baker. HPDP-biotin was from Thermo Scientific. N-ethylmaleimide was from Fluka. DTT was from Promega. *Escherichia coli* strain Rosetta (DE3) and vector pET15b were from Novagen. Human GAPDH (GenBank number BC029618) and human Triosephosphate isomerase (hTPI, GenBank number BC015100) cDNA clones were from Open Biosystems. HisTrap FF and PD SpinTrap G-25 columns were from GE Healthcare. Primary antibodies and horseradish peroxidase-conjugated secondary antibody were from Abcam and dye-labeled secondary antibodies were from LI-COR. S-nitrosoglutathione (GSNO) and S-nitrosocysteine (CySNO) were prepared as previously described [26]. Briefly, 40 mM l-glutathione or L-cysteine was incubated for 2 min in the dark with 80 mM $NaNO_2$ in 0.1 N HCl and the solutions were immediately used after neutralization with 0.2 vol of 0.5 M Tris base.

2.2. Human TPI mutagenesis, expression and purification

cDNA of hTPI was inserted into the expression vector pET15b, downstream of the His_6-tag encoding sequence of the plasmid. The resulting construct was used as template to generate hTPI-C217A mutant by site-directed mutagenesis utilizing the QuikChange site-directed mutagenesis kit (Stratagene, La Jolla, CA, USA). His_6-hTPI and C217A mutant were expressed in *Escherichia coli* strain Rosetta (DE3) and purified by affinity chromatography on HisTrap FF columns (1 mL). Fractions containing the protein were pooled, incubated with 10 mM DTT for 2 h at room temperature, desalted with HEN buffer (50 mM HEPES pH 7.7, 1 mM EDTA, and 0.1 mM neocuproine) and concentrated. Proteins concentrations were measured at 280 nm using 33460 $M^{-1} cm^{-1}$ molar extinction coefficient. hTPI and hTPI-C217A mutant (Fig. 1 A) were purified to apparent homogeneity according to SDS-PAGE analysis.

2.3. Determination of reduced cysteine residues

The reduced cysteine residues of hTPI accessible to solvent were assessed spectrophotometrically under non-denaturing conditions using 5,5′-dithiobis-(2- nitrobenzoic acid) (DTNB). Briefly, the absorbance at 412 nm of a mix containing 32 μM hTPI, 0.1 mM Tris–HCl pH 7.5 and 1 mM DTNB was measured up to 2 h and the thionitrobenzoate anion (TNB^-) concentration was determined using a 13600 $M^{-1} cm^{-1}$ molar extinction coefficient.

2.4. Incubation of hTPI with the NO-donors

hTPI was incubated with the indicated NO-donors in HEN buffer to prevent chemical denitrosylation. After incubation, the samples were processed for fluorometric assay, mass spectrometry, and western blot analysis of protein S-nitrosothiols as detailed below.

2.5. Detection of S-nitrosylated hTPI on western blots

S-nitrosylated hTPI was identified using the biotin-switch assay [27]. In brief, S-nitrosylated hTPI (150 μg) dissolved in HEN buffer containing 2% sodium dodecyl sulfate (SDS) was incubated with N-ethylmaleimide (NEM) to block free thiol groups. Thiol groups bound to NO were exposed to 3 mM ascorbic acid and titrated with HPDP-biotin in HEN buffer. Biotin-containing enzyme was separated by SDS-polyacrylamide gel electrophoresis (PAGE) and blotted to polyvinylidene fluoride (PVDF) membranes. Before western blot analysis, total transferred proteins were stained with Coomassie blue. Western blot analysis was performed with mouse polyclonal anti-biotin primary antibody and IRDye® 800 goat anti-mouse IgG secondary antibody using the Odyssey Infrared Imaging System (LI-COR, Lincoln, NE, USA). The fluorescent signals were quantified by densitometric analysis using IMAGEJ software (National Institutes of Health, Bethesda, MD, USA).

2.6. Fluorometric determination of NO-hTPI

Levels of NO-hTPI were assayed with a fluorometric technique [28]. Briefly, after S-nitrosylation NO-hTPI was separated from the excess NO-donors using PD SpinTrap G-25 columns. Aliquots corresponding to 50 μg of purified NO-hTPI were dissolved in 190 μL of 60 mM HCl containing 3.2 μM 2,3-diaminonaphthalene with and without 0.2 mM $HgCl_2$, and incubated at room temperature. After 10 min, 10 μL of 2.8 N NaOH was added to stabilize the fluorescent 2,3-naphthotriazole product. Fluorescence was measured using a FluoroMax-P fluorimeter (Horiba Jobin Yvon, Edison, NJ, USA) with excitation and emission wavelengths of 363 nm and 450 nm, respectively. Emission intensity was converted to NO-TPI concentration using a calibration curve generated by increasing amounts of sodium nitrite.

2.7. Mass spectrometry analysis

hTPI was incubated with CySNO for 1.5 or 3 h in order to obtain two NO-hTPI samples with different S-nitrosylation degree (0.41 ± 0.01 and 0.76 ± 0.06 mol S-NO/mole hTPI monomer, respectively). Non S-nitrosylated hTPI (control) and NO-TPI samples were purified by PD SpinTrap G-25 columns and incubated with 40 mM NEM, 2.5% SDS in HEN buffer, to block free SH groups. Excess NEM was removed by several acetone precipitations, the samples were incubated with 10 mM DTT and 1% SDS to reduce S-nitrosylated thiols and subjected to acetone precipitation once again to remove DTT and the protein pellets were then dried in a Speedvac at room temperature. Mass Spectrometry analysis of the precipitated protein was performed at the Proteomics Core Facility CEQUIBIEM, at the University of Buenos Aires/CONICET (National Research Council). Briefly, the samples were digested with 100 ng Trypsin (Promega V5111) in 25 mM ammonium bicarbonate pH 8 overnight at 37 °C. Peptides were desalted using C18 zip tips (Merck

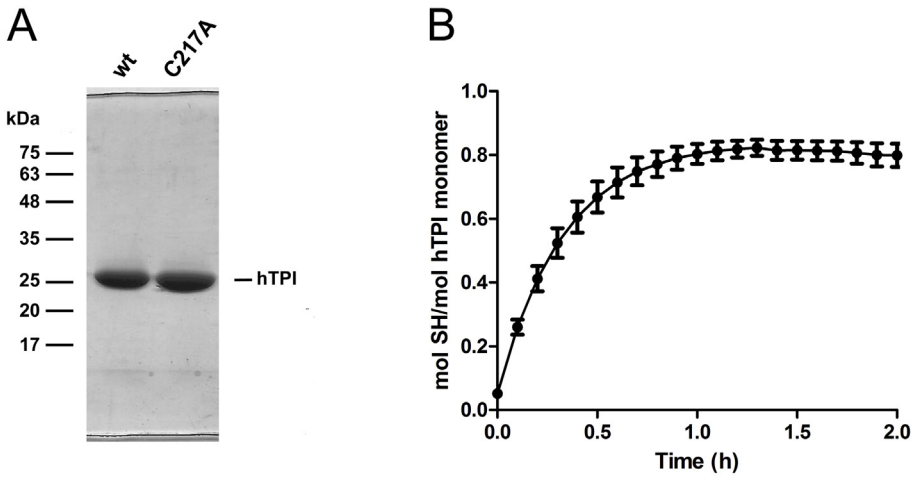

Fig. 1. A) SDS-PAGE of purified recombinant hTPI-wt and hTPI-C217A. 10 µg of wild type and mutant hTPI were subjected to SDS-PAGE and Coomassie blue stained. B) hTPI-cysteine accessibility to DTNB. Reduced hTPI cysteine thiols were quantified by absorption at 412 nm of the TNB produced during the indicated times. Values are the means ± SEM of triplicate determinations. (For interpretation of the references to colour in this figure legend, the reader is referred to the Web version of this article.)

Millipore) and eluted in 10 µL of water:acetonitrile:formic acid 40:60:0.1%. The digests were analyzed by nano LC-MS/MS in a nano HPLC EASY-nLC 1000 (Thermo Scientific) coupled to a QExactive Mass Spectrometer. A 75 min gradient of water:acetonitrile at a flow of 33 nl/min was used with a C18 2 mm Easy Spray column x 150 mm. Data Dependent MS2 method, was used to fragment the top 12 peaks in each cycle. The raw data from mass spectrometry analysis were processed using the Proteome Discoverer – version 2.1.1.21 – (Thermo Scientific) software for database searching with the SEQUEST search algorithm. Precursor mass tolerance was set to 10 ppm and product ion tolerance to 0.05 Da. Dynamic modifications were set to cysteine-sulfenate, cysteine-sulfinate, cysteine-sulfonate, and cysteine-alkylation by NEM. Hits were filtered for high confidence peptide matches with a maximum protein and peptide false discovery rate of 1% calculated by employing a reverse data base strategy.

2.8. Crystallization, data collection and structure determination

NO-hTPI was crystallized in 0.1 M HEPES pH 7.5, 20% PEG 4000, and 10% 2-propanol as previously described [29]. The crystals were grown using the hanging drop vapor diffusion method at 10 °C. The crystal was cryo-protected by soaking in a solution containing 70% mother liquor and 30% glycerol before being flash-frozen. Data were collected at the Protein Crystallography Beamline W01AMX2 of the Laboratório Nacional de Luz Síncrotron (LNLS), Campinas, Brazil (wavelength = 1.459 Å), at 100 K using a PILATUS 2M detector (Dectris). The data were processed and scaled using MOSFLM [30] and Scala [31], and subsequent analysis was performed using the CCP4 suite [32]. The crystal was isomorphous with the wild type hTPI crystal (PDB ID 2JK2) [18]. Thus, this structure without solvent molecules was used as a starting model for the refinement of the data, using the program REFMAC5 [33]. Positive difference electron density at Cys 217 in A subunit was interpreted as incomplete S-nitrosylation and modeled as *S*-nitrosocysteine (NO-Cys) with partial occupancy. This model was subjected to alternating cycles of refinement in REFMAC5 and manual inspection and model building with the program Coot [34]. Solvent molecules were added to the models in the final stages of refinement based on examination of difference density maps. The atomic coordinates and structure factors (code 6D43) have been deposited in Protein Data Bank (PDB).

2.9. hTPI activity assay

hTPI activity was measured in the direction of DHAP conversion to G3P. The reaction was coupled to purified recombinant hGAPDH [35] under conditions in which the overall reaction was limited by the isomerase reaction. The increase in the absorbance at 340 nm, due to the formation of NADH (extinction coefficient = 6220 M^{-1} cm^{-1}), was monitored at 30 °C using a Shimadzu UV-PC 1600 spectrophotometer equipped with a Peltier control of temperature. The incubation mixture contained 10 nM hTPI, 20 nM hGAPDH, 100 mM glycine, 100 mM NaH_2PO_4, 2 mM NAD^+, HEN buffer, and 0.1 mM–5 mM DHAP. All reactions were performed in triplicate. The initial rate was calculated over a DHAP range of concentrations and fit to the Michaelis-Menten equation in GraphPad Prism 5.0 software.

2.10. Statistical analysis

Results were analyzed for statistical significance with One-sample *t*-test utilizing GraphPad Prism 5.0 software.

3. Results

3.1. Accessibility of hTPI cysteine thiols

A first approach to determine the hTPI cysteine residues accessible to S-nitrosylation was carried out by calculating the accessible surface area (ASA) of these residues on hTPI 3D structures deposited in the Protein Data Bank (PDB ID 4POC, 1HTI, 1WYI and 2JK2) [18,29,36,37]. The results indicated that Cys86 was highly accessible followed by Cys66, with the others, Cys41, Cys126 and Cys217 showing poor accessibility (Table 1). This was in contrast with results reported by a proteomic analysis in human cells [19] which found S-nitrosylated Cys217, the residue with the lowest calculated ASA value. To explore the hTPI cysteines accessible to solvent, and hence able to be S-nitrosylated, the Ellman's reagent (DTNB) was used to titrate reduced thiols under non-denaturing conditions. The number of moles of free SH groups per mole of hTPI monomer was 0.81 ± 0.03 (n = 3, Fig. 1) a

Table 1
Accessible surface area (ASA) of hTPI-cysteine residues. Accessibility for the dimeric A and B subunits of the hTPI resolved structures (PDB ID 4POC, 1HTI, 1WYI, and 2JK2) was calculated with the AreaImol program from CCP4 package using a probe radius of 1.4 Å.

	ASA (Å^2)			
PDB ID:	4POC	1HTI	1WYI	2JK2
	Subunit A/B	Subunit A/B	Subunit A/B	Subunit A/B
Cys41	0.3/0.0	0.3/0.9	0.1/0.2	0.2/0.1
Cys66	1.2/1.4	0.6/0.7	1.4/1.9	1.2/1.4
Cys86	6.7/6.0	9.7/6.9	5.2/7.0	6.6/6.5
Cys126	0.1/2.7	0.5/0.3	0.0/0.1	0.0/0.1
Cys217	0.0/0.5	0.0/0.3	0.1/3.1	1.1/1.0

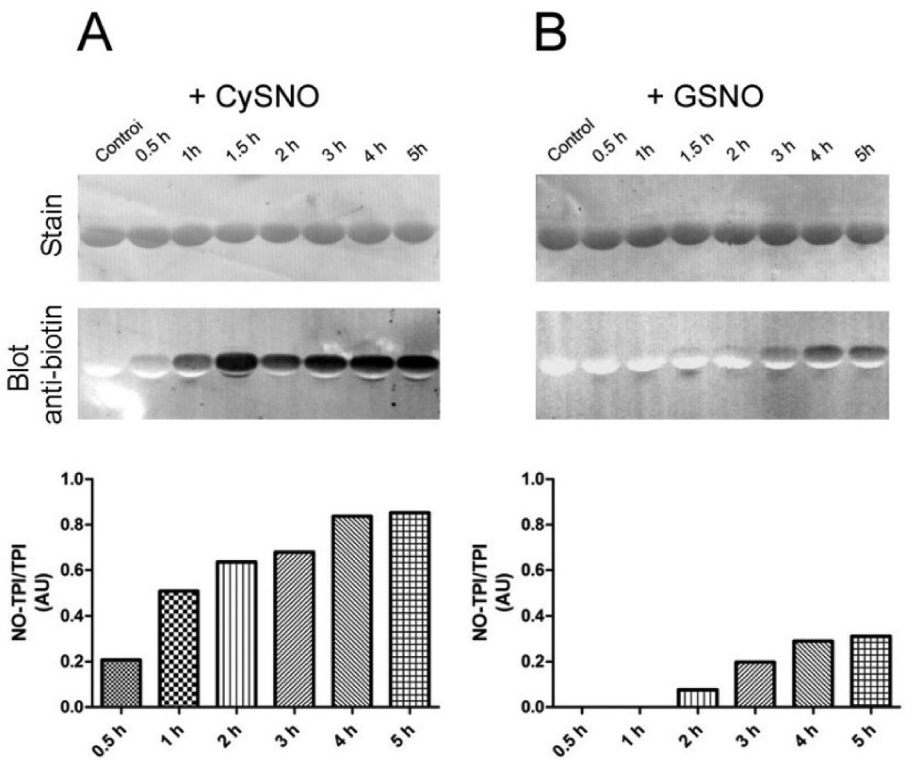

Fig. 2. S-nitrosylation of hTPI. hTPI (100 μM) was incubated for the indicated times with A) CySNO (10 mM) or B) GSNO (10 mM). NO-hTPI was detected by western blotting using the "biotin switch" method (see Materials and Methods). Relative levels of NO-TPI were also determined by scanning densitometry of western blots. Values are expressed as arbitrary units (AU) per total TPI (Coomassie blue stained band). Immunoblotting results are representative of three independent experiments. (For interpretation of the references to colour in this figure legend, the reader is referred to the Web version of this article.)

value that is about one-fifth of the SH groups determined in the presence of SDS (4.22 ± 0.04 mol SH/mole hTPI monomer, n = 11). This result suggests that only one of the five cysteine-thiol groups of each subunit was accessible to the reagent.

3.2. Mechanism and degree of hTPI S-nitrosylation

During this study, three different NO donors were used: CySNO, GSNO and Spermine NONOate (NONOate). CySNO and GSNO can potentially S-nitrosylate by two mechanisms. One is through N_2O_3, the main autooxidation product of the NO released by homolytic cleavage of the donor S-NO linkage. The other is S-transnitrosylation by the direct transfer of NO^+ to cysteinyl-SH groups. Instead, NONOate only releases free NO and therefore it S-nitrosylates thiol groups via N_2O_3. Using the biotin-switch method and western blot analysis, it was observed that CySNO and GSNO S-nitrosylated hTPI in a time-dependent manner while NONOate failed to modify the enzyme (Fig. 2 and Fig. 3 A). The N_2O_3-scavenger sodium azide was included in the S-nitrosylation assays in order to establish whether the modification was mediated by N_2O_3 or S-transnitrosylation. The presence of sodium azide did not affect the reaction produced by CySNO or GSNO, indicating that in both cases it occurred by S-transnitrosylation (Fig. 3 B). Quantitative fluorometric determination of NO-hTPI was carried out after removal of unreacted NO-donors by size-exclusion chromatography. The level of NO-hTPI generated by incubation of 100 μM hTPI with 10 mM CySNO was approximately 0.8 mol per mole of hTPI monomer in 3 h; a similar value was obtained at 20 h of incubation (Fig. 4), in accordance with the DTNB assay (Fig. 1). GSNO on the other hand produced about 0.4 mol S-NO/mole hTPI monomer at 3 h and at 20 h reached a similar level to that obtained by CySNO incubation (Fig. 4 A), indicating that both GSNO and CySNO were able to equally S-nitrosylate hTPI, the latter at a higher rate. These results are consistent with those of the biotin-switch assay shown in Fig. 2. However, incubation with 1 mM CySNO generated around 0.1 mol NO/mole hTPI monomer in 3 h while the use of 0.1 mM CySNO did not produce detectable amounts of NO-hTPI in the same incubation time (Fig. 4 B).

3.3. Mass spectrometry identification of hTPI S-nitrosylated cysteine

The identification of the modified cysteines by LC-MS/MS was performed through the analysis of Cys-NO-harboring peptides whose degree of abundance changed in accordance with a time-dependent S-

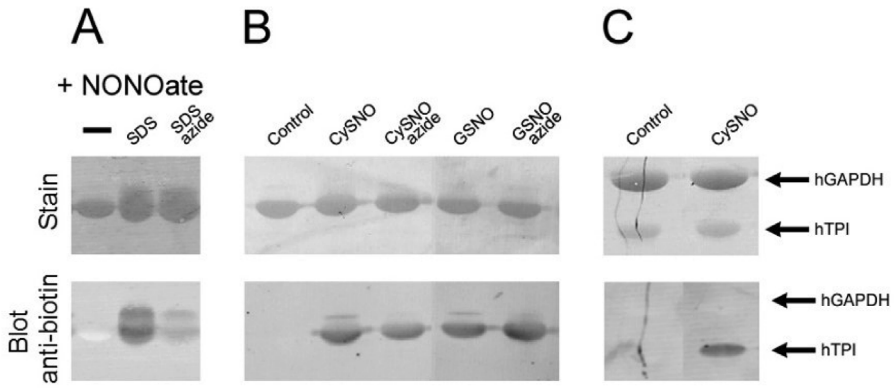

Fig. 3. S-nitrosylation in the presence of N_2O_3-scavenger and hGAPDH. A) hTPI (100 μM) was incubated for 3 h with the releasing NO donor NONOate (A), CySNO or GSNO (B) (all of them in a concentration of 10 mM) in the presence or absence of sodium azide (10 mM) and SDS (1%). In A), incubation of hTPI with NONOate (line 2) and NONOate plus sodium azide (lane 3) in presence of SDS were included as positive controls of NONOate reactivity and azide scavenger activity, respectively. C) hTPI (Control) and NO-hTPI (40 μM each) were incubated with 80 μM hGAPDH for 10 min at 30 °C and NO-bound protein determined by western blotting using the "biotin switch" method (see Materials and Methods). Immunoblotting results are representative of three independent experiments.

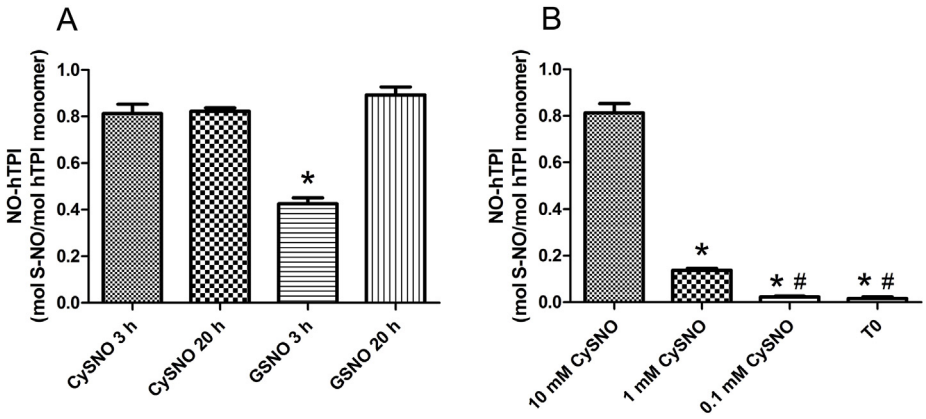

Fig. 4. Fluorometric determination of NO-hTPI. A) hTPI (100 μM) was incubated for 3 h or 20 h with 10 mM CySNO or GSNO, or B) incubated for 3 h with CySNO concentration indicated. Zero-time control was included (T0). The resultant NO-hTPI was determined by fluorometric assay (see Materials and Methods). Values represent the mean ± SEM of three separate experiments. *Significantly different ($P < 0.05$) from 10 mM CySNO 3 h #Significantly different ($P < 0.05$) from 1 mM CySNO.

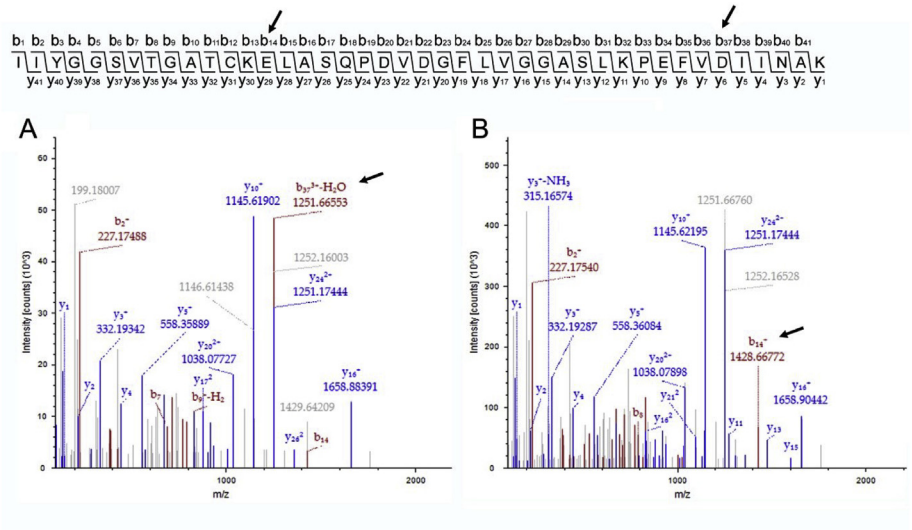

Fig. 5. Tandem mass spectra of the oxidized cysteine peptides. hTPI was S-nitrosylated with CySNO for 1.5 h or 3 h. The generated NO-hTPI was incubated with NEM to alkylate the non-S-nitrosylated thiols, and then with DTT to reduce the S-nitrosylated cysteines. The samples were digested with trypsin and the resulting peptides were analyzed by LC-MS/MS. Non-alkylated cysteines were detected in peptides containing Cys41, Cys126 and Cys217. Tandem mass spectra of Cys217-containig peptide from (A) 1.5 h and (B) 3 h hTPI S-nitrosylation are shown. The peptide ions that confirm non-alkylated cysteine are: $b37^{3+}$ (A) and $b14^{+}$ (B) (arrow). (C) Fractional amounts of non-alkylated peptide species. The chromatographic peak intensities of non-alkylated hTPI peptides and the corresponding alkylated peptides were obtained and the fractional amount of individual peptides species were calculated. The ionization efficiencies of all the peptide species were assumed to be the same.

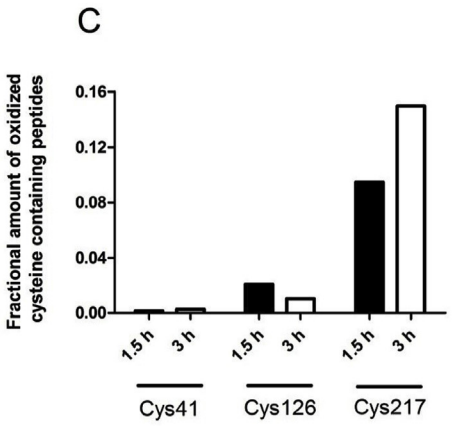

nitrosylation increase as shown in Fig. 2. For this purpose, samples were assayed as follow: NO-hTPI generated by incubation with CySNO for 1.5 h (0.41 ± 0.01 mol S-NO/mole hTPI monomer), and 3 h (0.76 ± 0.06 mol S-NO/mole hTPI monomer) were separated from unreacted NO-donor and incubated with NEM to alkylate the non S-nitrosylated thiols. Unmodified hTPI was processed in parallel as a control. After removal of the unreacted NEM, the samples were incubated with DTT to reduce those cysteine residues that were S-nitrosylated, washed by several acetone precipitations, digested with trypsin and analyzed by LC-MS/MS. The setting for cysteine-containing peptide identification involved residues alkylated by NEM and non-alkylated. The latter covered reduced-cysteine, sulfenate-cysteine, sulfinate-cysteine and sulfonate-cysteine since oxidation reactions may have occurred on reduced thiols during acetone precipitation. Only thiols alkylated with NEM were detected in peptides harboring the five cysteine residues in the control sample (data not shown). In S-nitrosylated samples, non-alkylated cysteines were found in peptides harboring Cys41, Cys126 and Cys217 (Fig. 5). In these cases cysteine-sulfinate or -sulfonate were detected. The analysis of the integrated chromatographic peak area values for individual oxidized peptides harboring either cysteine-sulfinate or cysteine-sulfonate, normalized by the sum of the integrated peak areas of those peptides both alkylated and oxidized, showed that Cys217 was the most abundant (Fig. 5 C) and the only peptide reflecting the expected increase in S-nitrosylation

Table 2
Data collection and refinement statistics.

Data set	NO-hTPI
Space group	P212121
a (Å)	64.92
b (Å)	73.98
c (Å)	93.80
Resolution Range (Å)	58.09–2.04 (2.09–2.04)
Observed reflections	131,346
Independent reflections	27,988
Rmerge (%)[a]	12.6 (30.1)
I/σ	3.3 (1.6)
Completeness (%)	95.2 (89.7)
Refinement	
Reflections in refinement	26,617
$R_{cryst.}$ (%)[b]	20.18
R_{free} (%) (test set 5%)[c]	25.63
r.m.s.d. on bond lengths (Å)[d]	0.008
r.m.s.d. on bond angles (°)[d]	1.286

The values in parentheses refer to the highest resolution shells.

[a] Rmerge = $\Sigma h \Sigma i \mid Iih - < Ih > \mid / \Sigma h \Sigma i < Ih >$, where $< Ih >$ is the mean intensity of the *i* observations of reflection *h*.

[b] Rcryst = Σ | |Fobs| - |Fcalc| |/Σ |Fobs|, where |Fobs| and |Fcalc| are the observed and calculated structure factor amplitudes, respectively. The summation includes all reflections used in the refinement.

[c] Rfree = Σ | |Fobs| - |Fcalc| |/Σ |Fobs|, evaluated for a randomly chosen subset of 5% of the diffraction data not included in the refinement.

[d] Root mean square deviation from ideal values.

levels among the samples subjected to 1.5 h and 3 h CySNO incubation (Fig. 5 C).

3.4. Crystal structure of NO-hTPI

To gain further insight into the modification sites, the NO-hTPI crystal structure was solved (Table 2). A dimeric form was present in the asymmetric unit and the overall structure was similar to other hTPI reported previously [18,29,36,37]. The fo – fc electron density map showed an extra electron density on Cys217 that was attributed to S-nitrosylation. Interestingly, the extra electron density was only observed in A protomer of the dimer (Fig. 6 A). After refinement, the final model showed S-nitrosylated and unmodified Cys217 in the A subunit, and unmodified Cys217 in the B subunit (Fig. 6 B). The electron density map around the other four cysteine residues was assigned to a free thiolate anion form (Fig. 7). The same result was observed in another hTPI crystal grown in a different precipitant solution that diffracted to a lower resolution (data not shown). It is worth mentioning that due to the labile nature of the S-NO bond, its breakdown during X-ray irradiation cannot be discarded. Although both subunits crystallized with the active site loop (residues 166–167) [38] in open conformation, the electron density map around these residues in B subunit is not clearly visible, suggesting mobility in this region (data not shown). Cys217 is located at approximately 20 Å from the active site. However, the oxygen atom of NO moiety of NO-Cys217 was positioned at 3.17 Å from the main chain amide nitrogen of Ile243 so as to allow hydrogen bonding. At the same time, Ile243 belongs to a helix-turn-helix motif harboring the residues Gly232 and Gly233 that interact with the phosphate moiety of DHAP (data not shown).

3.5. Effect of S-nitrosylation on hTPI enzymatic activity

In order to analyze the effect of S-nitrosylation on TPI activity, the Vo for hTPI and NO-hTPI with different concentrations of DHAP was determined (Fig. 8 A) and used for Vmax and Km calculation. Although no significant difference was observed in the Km, the Vmax of NO-hTPI

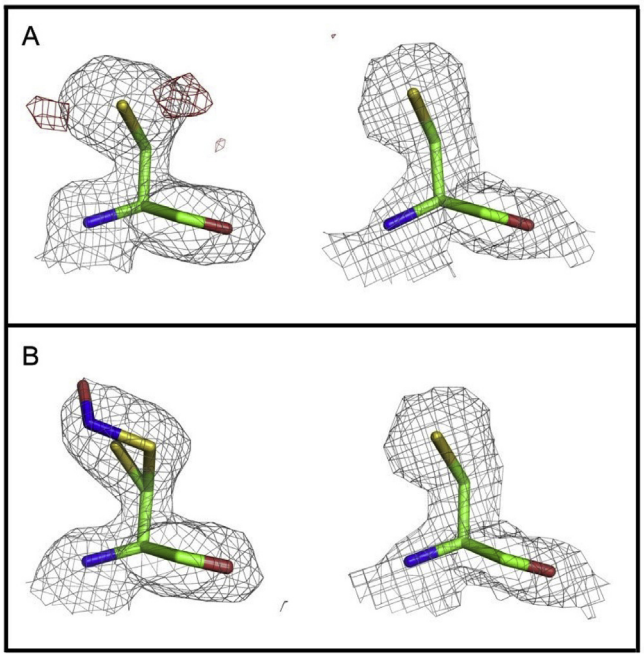

Fig. 6. Electron density maps showing the S-nitrosylation of Cys217 of NO-hTPI. (A) 2Fo − Fc electron density map in gray contoured at 1σ and Fo − Fc electron density map in red contoured at 2.4 σ for Cys217 of A subunit (left) and B subunit (right). (B) 2Fo − Fc electron density map after modeling the residue of A subunit as S-nitrosylated cysteine (left) and as thiolate for B subunit (right).

was 30% lower than that of the unmodified hTPI (Fig. 8 B, C). Since hGAPDH was part of the coupled enzyme assay used for hTPI activity determination, and it is known that GAPDH S-nitrosylation inhibits its activity, we discarded S-transnitrosylation between the two enzymes during the assay, since no NO-hGAPDH formation could be detected by the biotin switch assay (Fig. 3 C).

4. Discussion

Here we demonstrate for the first time that the *in vitro* S-nitrosylation of human TPI occurs by S-transnitrosylation from non-protein S-nitrosothiol mediators as CySNO and GSNO and not through N_2O_3, the autooxidation product of released NO. We have investigated the solvent accessibility of hTPI cysteines by ASA calculation from four reported X-ray crystal structures and by reaction with the cysteine-derivatizing reagent DTNB. The ASA calculation showed higher accessibility of Cys86 and, to a lesser extent to Cys66, while Cys41, Cys126 and Cys217 appeared to be poorly accessible. On the other hand, measurement of the wild type hTPI cysteines accessible to DTNB as well as the fluorometric quantification of NO-hTPI suggested that only one of the five cysteine-thiols was S-nitrosylated (Figs. 1 and 4). Though poorly accessible to the solvent according to the ASA calculation, Cys217 was nevertheless found to be S-nitrosylated by LC-MS/MS and X-ray diffraction (Figs. 6 and 7). A possible explanation for this discrepancy might be that conformational fluctuations of hTPI in solution could lead to exposure of Cys217, a dynamism restricted after crystal formation. In agreement with these results, Cys217 of hTPI was identified as a target of S-nitrosylation in a proteomic study carried out in human pulmonary arterial endothelial cell lysates [19].

Our LC-MS/MS study using purified NO-hTPI detected three peptides harboring Cys41, Cys126 and Cys217, respectively (Fig. 5). Semi-quantitative analysis showed that the peptide harboring Cys217 was the only one whose higher relative abundance increased in response to a higher degree of S-nitrosylation (Fig. 5). This increase together with the quantification of about 1 mol of S-NO per mole hTPI led us to consider Cys217 as the unique target of hTPI S-nitrosylation.

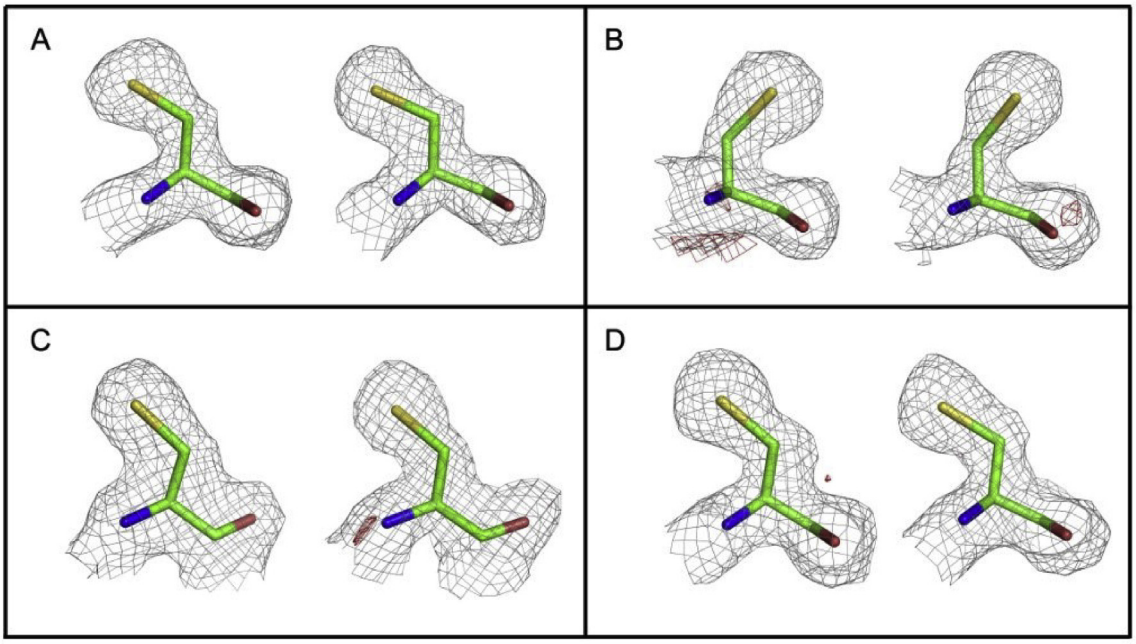

Fig. 7. 2Fo − Fc electron density map in gray contoured at 1σ and Fo − Fc electron density map in red contoured at 2.4 σ for (A) Cys41, (B) Cys66, (C) Cys86, and (E) Cys126 of A subunit (left) and B subunit (right).

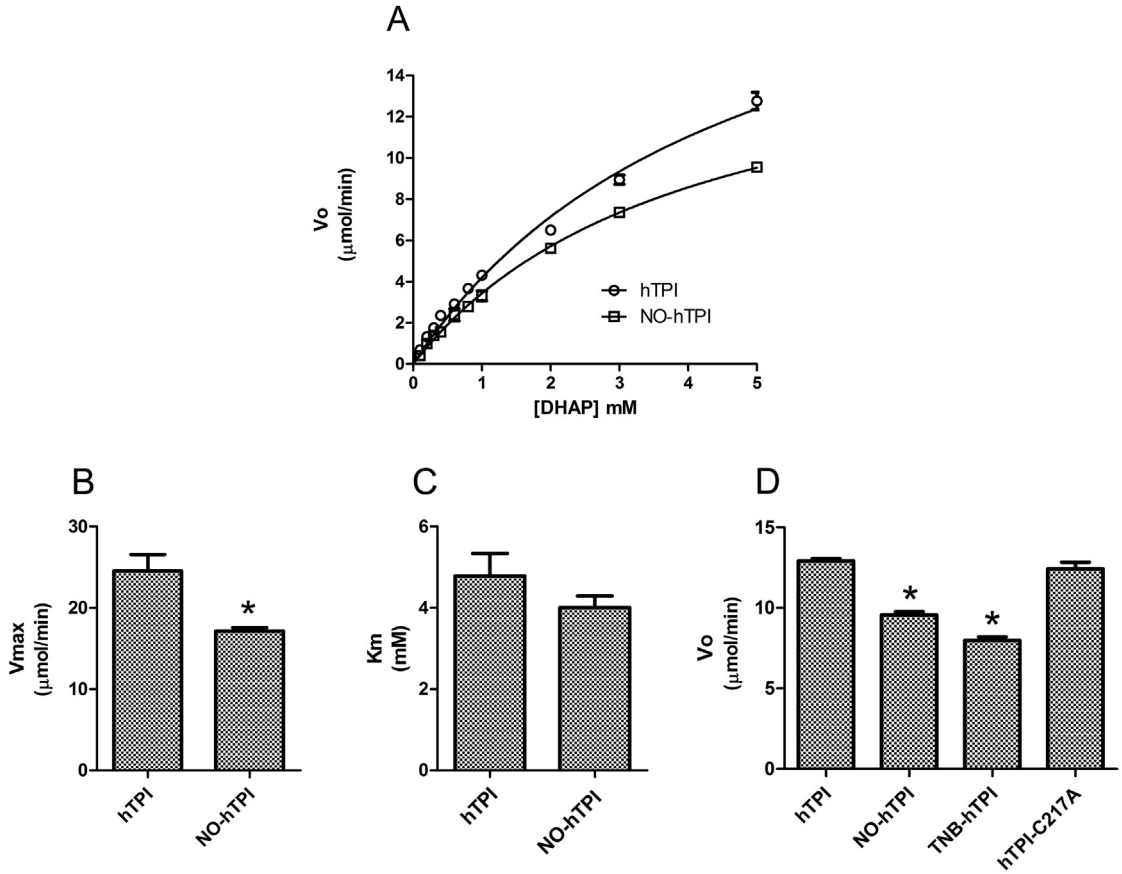

Fig. 8. Effect of S-nitrosylation on hTPI activity. A) Michaelis-Menten kinetic profiles. hTPI was incubated with CySNO and the initial reaction rate (Vo) was determined for the indicated DHAP concentrations. B) Vmax and C) DHAP Km were calculated by fitting with the Michaelis–Menten equation using nonlinear regression in GraphPad Prism 5.0b (GraphPad Software). D) Initial velocity (Vo) with 5 mM DHAP of hTPI, NO-hTPI, TNB-hTPI and hTPI-C217A mutant. Values are the means ± SEM of triplicate determinations. *Significantly different ($P < 0.05$) from hTPI.

Interestingly, despite the fact that the S-nitrosylation quantification assay yielded around 1 mol S-NO/mole hTPI monomer, the crystal structure of NO-hTPI revealed that the S-nitrosylation was observed only in Cys217 of the A subunit of the dimer. It is not known whether the NO-Cys217 of B subunit was decomposed during protein crystallization or X-ray irradiation. This asymmetric phenomenon was observed in the other hTPI structures. As mentioned before, there are four wild-type hTPI structures deposited in the PDB. Three of them crystallized with the active site loop in different conformations between the A and B subunits (1HTI, 1WYI, 4POC) and with a substrate analog bound only to one subunit in two cases (4POC and 1HTI). It has been speculated that in solution, some dimers are composed of conformationally asymmetric subunits, causing substrate binding in only one of them [39]. Differences in crystal growth intake rates between dimers with conformationally symmetric and asymmetric subunits could therefore favor the crystallization of the second one. In solution, the S-nitrosylation could be either favored or more stable in only one subunit of a dimer with conformationally asymmetric subunits, this dimer possibly being the crystallized species as mentioned before.

Though none of the five cysteine residues are directly involved in the catalytic site, this does not exclude them from a potentially important role in enzyme function. Amino acids not involved in the catalytic site, but essential for hTPI function were discovered during studies on TPI deficiency. TPI deficiency is a rare genetic disease characterized by a decrease in enzyme activity in all the tissues studied, causing hemolytic anemia and neurological disorder frequently leading to death in early childhood [40,41]. From eleven missense mutations described, nine occur on residues that do not show a direct relationship with the catalytic site when analyzed in the static models of wild-type hTPI obtained by X-ray crystallography [40]. However, these mutations induced impairment of hTPI function. Some of them are located near the dimer interface, and were therefore proposed to alter dimer stability [40,42].

We found that hTPI S-nitrosylation produced approximately 30% inhibition in Vmax (25% inhibition in Vo with 5 mM DHAP, Fig. 8 D), while Km for DHAP was not significantly modified. As shown in Fig. 1 B, DTNB reacted with one cysteine residue of hTPI to form TNB^- and TNB-hTPI. This modification reduced the Vo around 37% (Fig. 8 D), the same order than S-nitrosylation. This inhibitory effect can be attributed to TNB-hTPI species since intermolecular disulfide hTPI species were not found in non-reducing SDS-PAGE analysis (result not shown). In order to evaluate the role of Cys217 in hTPI activity, the hTPI-C217A mutant was generated by site-directed mutagenesis. The amount of cysteine accessible to solvent of hTPI-C217A determined with Ellman's reagent was around 10% of the value found for hTPI (0.082 ± 0.004 mol SH/mole hTPI-C217A monomer, $n = 3$) and the level of NO-hTPI-C217A measured by a fluorometric method was the same as the background (T0, data not shown) confirming that Cys217 is the main target of S-nitrosylation. However, the Vo with 5 mM DHAP of the mutant was the same as that determined with hTPI (Fig. 8 D). These results suggest that the inhibitory effect could be due to NO moiety presence instead of absence of Cys217 thiol. Some inhibition was also observed in the S-nitrosylated *Chlamydomonas reinhardtii* TPI [21]. It is not yet known whether this attenuation in activity could affect the glycolysis rate. In this connection it was reported that a 37% inhibition of GAPDH activity in reperfused myocardial tissue produced a twofold elevation in G3P concentration and reduction in the glucose metabolic rate [43]. As in the NO-hTPI case, no change in the Km of GAPDH for G3P was observed. This inhibition could be caused by covalent modification of GAPDH by reactive oxygen/nitrogen species during reperfusion. Therefore, in addition to the effect of GAPDH activity inhibition, the possibility that S-nitrosylated hTPI activity inhibition contributes to glycolysis impairment during oxidative/nitrosative damage cannot be discarded.

Cys217 is located far from the dimer interface and at around 20 Å from the active site. However, the DHAP phosphate moiety interacting residues, Gly232 and Gly233 [29], are part of a helix-turn-helix motif where Ile243 is also located. Ile243 main chain amide nitrogen would form a hydrogen bond with the oxygen atom of NO of NO-Cys217. Although S-nitrosylation of hTPI did not affect Km for DHAP, more studies will be necessary to ascertain whether this interaction could have any effect on the enzyme activity.

The amount of biosynthesized NO depends on the physiological event. During inflammatory processes, large amounts of NO are released from macrophages upon iNOS activation [2,3]. It is believed that the way to spread NO is through non-protein S-nitrosothiols as CySNO and/or GSNO [9,26]. Here we show that CySNO is more effective than GSNO for hTPI S-nitrosylation. Thiol accessibility and interaction between donor and thiol target might be determining factors behind this preference, suggesting that CySNO could be considered the NO-donor of election in future studies related to the effect of NO on hTPI in cellular environments.

In conclusion, we have investigated how hTPI is S-nitrosylated, which cysteine residue is modified, and how it affects the enzyme activity. This study is relevant to understanding the effects that nitrosative stress may have on a key enzyme of the glycolytic pathway.

Funding

This work was supported by grants from Consejo Nacional de Investigaciones Científicas y Técnicas, Fondo para la Investigación Científica y Tecnológica and Secretaría de Ciencia y Técnica-Universidad Nacional de Córdoba (SECyT-UNC).

Acknowledgments

We thank Phyllis Barrantes for English revision of the manuscript. We acknowledge the LNLS for provision of synchrotron radiation facilities and Alexandre Lo Bianco dos Santos for assistance in using beamline W01AMX2. We also acknowledge the Proteomics Core Facility CEQUIBIEM, at the University of Buenos Aires/CONICET and Dr. Silvia Moreno for her help in processing mass spectrometer data.

References

[1] R.G. Knowles, S. Moncada, Nitric oxide synthases in mammals, Biochem. J. 298 (1994) 249–258.
[2] J.F. Parkinson, B. Mitrovic, J.E. Merrill, The role of nitric oxide in multiple sclerosis, J. Mol. Med. (Berl.) 75 (1997) 174–186.
[3] A.J. Duncan, S.J. Heales, Nitric oxide and neurological disorders, Mol. Aspect. Med. 26 (2005) 67–96.
[4] J.S. Stamler, Redox signaling: nitrosylation and related target interactions of nitric oxide, Cell 78 (1994) 931–936.
[5] M.C. Broillet, S-nitrosylation of proteins, Cell. Mol. Life Sci. 55 (1999) 1036–1042.
[6] D.R. Arnelle, J.S. Stamler, NO+, NO, and NO- donation by S-nitrosothiols: implications for regulation of physiological functions by S-nitrosylation and acceleration of disulfide formation, Arch. Biochem. Biophys. 318 (1995) 279–285.
[7] A.R. Butler, F.W. Flitney, D.L. Williams, NO, nitrosonium ions, nitroxide ions, nitrosothiols and iron-nitrosyls in biology: a chemist's perspective, Trends Pharmacol. Sci. 1 (1995) 18–22.
[8] T. Akaike, Mechanisms of biological S-nitrosation and its measurement, Free Radic. Res. 5 (2000) 461–469.
[9] Y. Zhang, N. Hogg, Formation and stability of S-nitrosothiols in RAW 264.7 cells, Am. J. Physiol. 287 (2004) L467–L474.
[10] J.S. Beckman, W.H. Koppenol, Nitric oxide, superoxide, and peroxynitrite: the good, the bad, and ugly, Am. J. Physiol. 271 (1996) C1424–C1437.
[11] A.H. Cross, P.T. Manning, M.K. Stern, T.P. Misko, Evidence for the production of peroxynitrite in inflammatory CNS demyelination, J. Neuroimmunol. 80 (1997) 121–130.
[12] J.S. Liu, M.L. Zhao, C.F. Brosnan, S.C. Lee, Expression of inducible nitric oxide synthase and nitrotyrosine in multiple sclerosis lesions, Am. J. Pathol. 158 (2001) 2057–2066.
[13] O.A. Bizzozero, G. DeJesus, T.A. Howard, Exposure of rat optic nerves to nitric oxide causes protein S-nitrosation and myelin decompaction, Neurochem. Res. 29 (2004) 1675–1685.
[14] T.M. Greco, R. Hodara, I. Parastatidis, H.F. Heijnen, M.K. Dennehy, D.C. Liebler, H. Ischiropoulos, Identification of S-nitrosylation motifs by site-specific mapping of the S-nitrosocysteine proteome in human vascular smooth muscle cells, Proc. Natl. Acad. Sci. U. S. A 103 (2006) 7420–1425.
[15] G.C. Brown, Nitric oxide and mitochondria, Front. Biosci. 12 (2007) 1024–1033.

[16] Y. Sha, H.E. Marshall, S-nitrosylation in the regulation of gene transcription, Biochim. Biophys. Acta 1820 (2012) 701–711.
[17] H. Takahashi, Y. Shin, S.J. Cho, W.M. Zago, T. Nakamura, Z. Gu, Y. Ma, H. Furukawa, R. Liddington, D. Zhang, G. Tong, H.S. Chen, S.A. Lipton, Hypoxia enhances S-nitrosylation-mediated NMDA receptor inhibition via a thiol oxygen sensor motif, Neuron 53 (2007) 53–64.
[18] C. Rodríguez-Almazán, R. Arreola, D. Rodríguez-Larrea, B. Aguirre-López, M.T. de Gómez-Puyou, R. Pérez-Montfort, M. Costas, A. Gómez-Puyou, A. Torres-Larios, Structural basis of human triosephosphate isomerase deficiency: mutation E104D is related to alterations of a conserved water network at the dimer interface, J. Biol. Chem. 283 (2008) 23254–23263.
[19] C.I. Murray, H. Uhrigshardt, R.N. O'Meally, R.N. Cole, J.E. Van Eyk, Identification and quantification of S-nitrosylation by cysteine reactive tandem mass tag switch assay, Mol. Cell. Proteomics 11 (2012) M111.013441.
[20] P.T. Doulias, J.L. Greene, T.M. Greco, M. Tenopoulou, S.H. Seeholzer, R.L. Dunbrack, H. Ischiropoulos, Structural profiling of endogenous S-nitrosocysteine residues reveals unique features that accommodate diverse mechanisms for protein S-nitrosylation, Proc. Natl. Acad. Sci. U. S. A 107 (2010) 16958–16963.
[21] M. Zaffagnini, L. Michelet, C. Sciabolini, N. Di Giacinto, S. Morisse, C.H. Marchand, P. Trost, S. Fermani, S.D. Lemaire, High-resolution crystal structure and redox properties of chloroplastic triosephosphate isomerase from *Chlamydomonas reinhardtii*, Mol. Plant 7 (2014) 101–120.
[22] C. Lindermayr, G. Saalbach, J. Durner, Proteomic identification of S-nitrosylated proteins in Arabidopsis, Plant Physiol. 137 (2005) 921–930.
[23] G. Tanou, P. Filippou, M. Belghazi, D. Job, G. Diamantidis, V. Fotopoulos, A. Molassiotis, Oxidative and nitrosative-based signaling and associated post-translational modifications orchestrate the acclimation of citrus plants to salinity stress, Plant J. 72 (2012) 585–599.
[24] G. Tanou, C. Job, M. Belghazi, A. Molassiotis, G. Diamantidis, D. Job, Proteomic signatures uncover hydrogen peroxide and nitric oxide cross-talk signaling network in citrus plants, J. Proteome Res. 9 (2010) 5994–6006.
[25] A. Lin, Y. Wang, J. Tang, P. Xue, C. Li, L. Liu, B. Hu, F. Yang, G.J. Loake, C. Chu, Nitric oxide and protein S-nitrosylation are integral to hydrogen peroxide-induced leaf cell death in rice, Plant Physiol. 158 (2012) 451–464.
[26] J.M. Romero, O.A. Bizzozero, Extracellular S-nitrosoglutathione, but not S-nitrosocysteine or N(2)O(3), mediates protein S-nitrosation in rat spinal cord slices, J. Neurochem. 99 (2006) 1299–1310.
[27] S.R. Jaffrey, S.H. Snyder, The biotin switch method for the detection of S-nitrosylated proteins, Sci. STKE 86 (2001) pl1.
[28] J.K. Park, P. Kostka, Fluorometric detection of biological S-nitrosothiols, Anal, Biochemist 249 (1997) 61–66.
[29] S.C. Mande, V. Mainfroid, K.H. Kalk, K. Goraj, J.A. Martial, W.G. Hol, Crystal structure of recombinant human triosephosphate isomerase at 2.8 A resolution. Triosephosphate isomerase-related human genetic disorders and comparison with the trypanosomal enzyme, Protein Sci. 3 (1994) 810–821.
[30] A.G.W. Leslie, Recent changes to the MOSFLM package for processing film and image plate data Jnt. CCP4/ESF-EACMB, Newslett. Protein Crystallogr 26 (1992) 27–33.
[31] P.R. Evans, Scaling and assessment of data quality, Acta Crystallogr. D Biol. Crystallogr 62 (2006) 72–82.
[32] M.D. Winn, C.C. Ballard, K.D. Cowtan, E.J. Dodson, P. Emsley, P.R. Evans, R.M. Keegan, E.B. Krissinel, A.G. Leslie, A. McCoy, Overview of the CCP4 suite and current developments, Acta Crystallogr. D Biol. Crystallogr 67 (2011) 235–242.
[33] G.N. Murshudov, A.A. Vagin, E.J. Dodson, Refinement of macromolecular structures by the maximum-likelihood method, Acta Crystallogr. D Biol. Crystallogr 53 (1997) 240–255.
[34] P. Emsley, B. Lohkamp, W.G. Scott, K. Cowtan, Features and development of Coot, Acta Crystallogr. D Biol. Crystallogr 66 (2010) 486–501.
[35] M.C. González, J.M. Romero, M.C. Ingaramo, C.J. Muñoz, J.A. Curtino, M.E. Carrizo, Enhancement by GOSPEL protein of GAPDH aggregation induced by nitric oxide donor and its inhibition by NAD, FEBS Lett. 590 (2016) 2210–2220.
[36] T. Kinoshita, R. Maruki, M. Warizaya, H. Nakajima, S. Nishimura, Structure of a high-resolution crystal form of human triosephosphate isomerase: improvement of crystals using the gel-tube method, Acta Crystallog. Sect. F. Struct. Biol. Cryst. Commun 61 (2005) 346–349.
[37] B.P. Roland, C.G. Amrich, C.J. Kammerer, K.A. Stuchul, S.B. Larsen, S. Rode, A.A. Aslam, A. Heroux, R. Wetzel, A.P. VanDemark, M.J. Palladino, Triosephosphate isomerase I170V alters catalytic site, enhances stability and induces pathology in a Drosophila model of TPI deficiency, Biochim. Biophys. Acta 1852 (2015) 61–69.
[38] F. Massi, C. Wang, A.G. Palmer, Solution NMR and computer simulation studies of active site loop motion in triosephosphate isomerasa, Biochemistry 45 (2006) 10787–10794.
[39] R. Aparicio, S.T. Ferreira, I. Polikarpov, Closed conformation of the active site loop of rabbit muscle triosephosphate isomerase in the absence of substrate: evidence of conformational heterogeneity, J. Mol. Biol. 334 (2003) 1023–1041.
[40] F. Orosz, J. Oláh, J. Ovádi, Triosephosphate isomerase deficiency: new insights into an enigmatic disease, Biochim. Biophys. Acta 1792 (2009) 1168–1174.
[41] A.S. Schneider, Triosephosphate isomerase deficiency: historical perspectives and molecular aspects, Baillieres Best Pract. Res. Clin. Haematol 1 (2000) 119–140.
[42] C. Oliver, D.J. Timson, In silico prediction of the effects of mutations in the human triose phosphate isomerase gene: towards a predictive framework for TPI deficiency, Eur. J. Med. Genet. 60 (2017) 289–298.
[43] R.J. Knight, K.F. Kofoed, H.R. Schelbert, D.B. Buxton, Inhibition of glyceraldehyde-3-phosphate dehydrogenase in post-ischaemic myocardium, Cardiovasc. Res. 32 (1996) 1016–1023.